# Egomotion Estimation Using Log-Polar Images

César Silva* José Santos-Victor
Instituto de Sistemas e Robótica - Instituto Superior Técnico,
Av. Rovisco Pais, 1096 Lisboa Codex, PORTUGAL
e-mail: {cesar,jasv}@isr.ist.utl.pt

**Abstract**

*We address the problem of egomotion estimation of a monocular observer moving with arbitrary translation and rotation in an unknown environment, using log-polar images.*

*The method we propose is uniquely based on the spatio-temporal image derivatives, or the normal flow. Thus, we avoid computing the complete optical flow field, which is an ill-posed problem due to the aperture problem. We use a search paradigm based on geometric properties of the normal flow field, and consider a family of search subspaces to estimate the egomotion parameters. These algorithms are particularly well-suited for the log-polar image geometry, as we use a selection of special normal flow vectors with simple representation in log-polar coordinates. This approach highlights the close coupling between algorithmic aspects and the sensor geometry (retina physiology), often found in nature.*

*Finally, we present and discuss a set of experiments, for various kinds of camera motions, which show encouraging results.*

## 1 Introduction

We address the problem of egomotion estimation for a monocular moving observer, using space-variant (log-polar) sampled images.

Recently, some vision systems have used non-uniform image sampling mechanisms, such as log-polar images[12, 2, 4]. The main advantages of using space-variant sampled images are related to perceptual and algorithmic complexity issues. The log-polar images are smaller than the cartesian images, providing an important data reduction, and contain a foveal area defining a focus of attention. Additionally this image geometry seems more suited than cartesian images for certain vision tasks like binocular vergence [2] and, as we will show, egomotion estimation.

The problem of egomotion estimation consists in determining the 3D motion parameters, by observing an image sequence over time. The first step to estimate egomotion or structure from motion is the computation of displacement between consecutive frames. Usual approaches are based either on point correspondences [9]; on the estimation of the dense motion field, identified by the optical flow [6, 4]; or the so-called direct methods [8, 5].

The correspondence problem or the full optical flow estimation are, in general, ill-posed [1, 3], and it is usually necessary to introduce very restrictive assumptions about the observed scenes. The solutions obtained often require large amounts of computation. The direct methods are less demanding than the previous ones, and use the image brightness information directly to recover the motion parameters, often based on normal flow or the spatio-temporal image derivatives. Here we focus the approach developed by Fermuller and Aloimonos [5] who introduced a method which is based on a selection of image points that form global patterns in the image plane, using the orientation of global normal flow vectors. This approach considers the egomotion estimation problem as a pattern recognition problem, introducing a set of geometric constraints that reveal a global structure hidden in the normal flow fields.

The approach we propose extends previous work described in [10, 11]. The method consists in searching the image for particular geometric properties of the normal flow, measured on the log-polar plane, tightly connected to the egomotion parameters. Hence, rather than considering the whole set of image flow data, the method uses a set of normal flow vectors with particular orientations and exploits a number of geometric constraints of the normal flow field. Both the selected flow vectors and the geometric constraints have a natural and simple representation in log-polar coordinates. Hence, one can benefit from using a sensor geometry which is particularly well adapted to the visual problem to be solved.

In Section 2, we introduce the main aspects related to log-polar transformation. Section 3 presents the optic flow and describe the model equations to be used throughout the paper. Section 4 is devoted to the proposed egomotion estimator. We define a set of constrained search algorithms for log-polar images, which represent the global estimation framework. Section 5 describes the experiments done, using both synthetic and real images. Finally, in Section 6 we draw some conclusions and establish further directions of work.

## 2 Log-Polar Mapping

The real-time control of vision systems imposes constraints on the computational complexity of the egomotion estimation algorithms. In this paper, we

*César Silva supported by a grant from PRAXIS-XXI research program. This work was partially funded by projects PRAXIS/3/3.1/TPR/23/94 and JNICT-PBIC/TPR/2550/95.

illustrate that egomotion estimation from normal flow can be achieved at very reduced computational cost using log-polar images.

In the human vision system, the retina has a space-variant distribution of photo-sensitive elements, with increasing density towards the center. Similarly, the log-polar images exhibit higher resolution at the center whereas the peripheral visual field is covered with a coarser resolution. The log-polar mapping is a rotationally symmetric transformation, which implicitly defines a foveal region in the retina and allows to concentrate the computational effort on the focus of attention, thus reducing the required amount of computations. The log-polar mapping [12] from a point $(x, y)$ on the cartesian plane to a point $(\lambda, \gamma)$ on the log-polar plane, is given by:

$$\begin{cases} \lambda = \log_l r \\ \gamma = \psi \end{cases} \tag{1}$$

where $l$ is the logarithmic factor and $(x, y) = r(\cos\psi, \sin\psi)$ as usual. The log-polar transformation has a singularity in the origin, avoided by limiting the range of $\lambda \in [\log_l r_{min},\ \log_l r_{max}]$, where $r_{max}$ depends on the cartesian plane dimensions, and $r_{min}$ describes the neighborhood of the origin where the transformation is not defined.

Figure 1 shows the original cartesian plane and the corresponding log-polar plane. As an illustration of

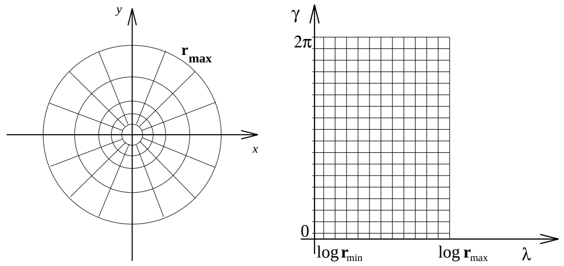


Figure 1: Log-polar transformation. Left: Cartesian image. Right Log-polar representation.

the log-polar mapping, Figure 2 shows the mapping of a cartesian image, and illustrates the main characteristics of the log-polar mapping. Firstly, there is an important data reduction (8 times) while the information content of the images is still sufficient to perceive its structure. Secondly, there is high resolution at the center and low resolution at the image periphery.

## 3 Problem Statement

Throughout the paper, we consider a camera-centered coordinate system. The image formation is modeled as a perspective projection. Given the camera linear velocity $\mathbf{t} = [U\ V\ W]^T$, angular velocity $\boldsymbol{\omega} = [\omega_1\ \omega_2\ \omega_3]^T$, the focal length $f$, and the scene depth at each point, $Z$, the motion field induced on the image plane, can be calculated at every pixel by the following well-known vector equation [6] :

$$\mathbf{v}(\mathbf{x}) = \rho(\mathbf{x})(\mathbf{x} - \boldsymbol{\Sigma}) + \mathbf{B}(\mathbf{x})\boldsymbol{\omega} \tag{2}$$

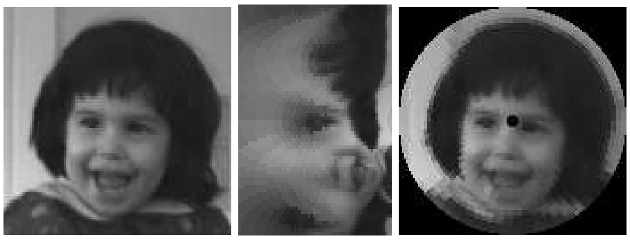

Figure 2: The original cartesian image (left) is mapped into log-polar representation (center). On the right, the image is remapped back to the cartesian plane.

where $\mathbf{v}(\mathbf{x}) = [u(\mathbf{x})\ v(\mathbf{x})]^T$ is the optical flow observed at a given image site, $\mathbf{x} = [x\ \ y]^T$; $\boldsymbol{\Sigma} = [\sigma\ \ \eta]^T = [fU/W, fV/W]^T$ is the Focus of Expansion (FOE) and corresponds to the projection of the observer linear velocity, $\mathbf{t}$, in the image plane. The function $\rho(\mathbf{x})$ is the inverse of the time-to-crash, given by $\rho(x, y) = W/Z(x, y)$. The rotation is multiplied by:

$$\mathbf{B}(\mathbf{x}) = \begin{bmatrix} \frac{xy}{f} & -(\frac{x^2}{f} + f) & y \\ (\frac{y^2}{f} + f) & -\frac{xy}{f} & -x \end{bmatrix} \tag{3}$$

We conclude from equation (2) that the component of the flow due to translation radiates from the FOE, thus lying on the lines that contain the FOE.

Heeger and Jepson [6] propose to recover the FOE using the complete optical flow field. They observed that given the FOE location, $\boldsymbol{\Sigma}$, equation (2) is linear in the remaining variables, $\boldsymbol{\omega}$ and $\rho$. The problem can be solved with $N > 3$ points, with a least mean squares estimator. The equations are solved for a set of $\boldsymbol{\Sigma}$ candidate points, computing the respective residual error. Naturally, for the correct FOE the residue should be minimal. However, this method is based on computationally demanding search algorithms and does not take into account the aperture problem constraint.

Due to the well-known constraint of the aperture problem [7], we can only observe the projection of the optical flow, $\mathbf{v}$, on the direction of the image gradient, $\mathbf{n}$. At each image point, the *normal-flow*, $v_n = \mathbf{n} \cdot \mathbf{v}$, provides a single constraint on the unknown components of the flow; and the estimation problem proposed above cannot be solved.

To overcome this problem we can eliminate the dependency on $\rho(\mathbf{x})$ (or equivalently the dependency on depth). If, for each $\boldsymbol{\Sigma}$, instead of using the flow all over the image, we select only the image sites, where the normal flow does not have translational component, then the aperture problem is no longer a limitation. These special vectors correspond to the set of normal flow vectors that are perpendicular to a line joining the image point and the FOE (i.e. $\mathbf{n} \cdot (\mathbf{x} - \boldsymbol{\Sigma}) = \mathbf{0}$). The nature of these vectors suggests the need of a more general study on geometrical properties of the normal flow field in order to improve the corresponding egomotion algorithm [5, 11]. In our study, we focus on a special set of properties of special subsets of the normal flow field, the *radial* and *circular* normal flow vectors, that have a very simple representation in the log-polar domain.

# 4 Egomotion Estimation

Next we analyze the special image sites where the contributions of the camera translation and rotation to the radial and circular normal flow are decoupled, in order to estimate the motion parameters separately.

## 4.1 Geometrical properties of the radial and circular normal flow

The *radial normal flow* is defined as the set of normal flow vectors with radial directions, $\mathbf{n_r}$. Let us consider the subset of the radial normal flow vectors that fulfill the following additional constraint: $\mathbf{n_r} \cdot (\mathbf{x} - \mathbf{\Sigma}) = 0$. For these image sites, the radial normal flow is also perpendicular to lines going through the FOE and therefore, does not depend on the camera translation (see equation (2)). We can identify the loci of these image points, by using polar coordinates ($x = r\cos\psi,\ y = r\sin\psi$):

$$(\cos\psi, \sin\psi) \cdot (r\cos\psi - \sigma, r\sin\psi - \eta) = 0$$
$$\Leftrightarrow \quad r = (\sigma, \eta) \cdot (\cos\psi, \sin\psi) \qquad (4)$$

Hence, these image points describe a circle (the **Γ-circle**) having the image center and the FOE, $(\sigma, \eta)$ as diametrical opposite points, as shown in Figure 3a. We can examine the influence of the camera rotation on the radial normal flow. The rotational component, $v_r$, of the radial normal flow can be written in polar coordinates:

$$v_r = \left(\frac{r^2}{f} + f\right)(\omega_1, \omega_2) \cdot (\sin\psi, -\cos\psi) \qquad (5)$$

Then, the rotational component of the radial normal flow has a sinusoidal behavior in $\psi$ for a fixed radius, $r$, and vanishes along a line defined by the image origin and the AOR, $\left(f\frac{\omega_1}{\omega_3}, f\frac{\omega_2}{\omega_3}\right)$, as shown in Figure 3a.

Similarly we can analyze the *circular normal flow* defined as the set of normal flow vectors with a direction $\mathbf{n_c}$, perpendicular to radial lines. We may consider the subset of the *circular normal flow* field, that verifies: $\mathbf{n_c} \cdot (\mathbf{x} - \mathbf{\Sigma}) = 0$. For all these points, the circular normal flow is also perpendicular to lines going through the FOE and therefore, does not depend on the camera translation (see Figure 3b). We can identify these special image sites, by using polar coordinates again:

$$(\sigma, \eta) \cdot (\sin\psi, -\cos\psi) = 0 \qquad (6)$$

Hence, this is the equation of a line (the **Ψ-line**) defined by the FOE, and the image center. Furthermore, the rotational component of the circular normal flow vectors is given by :

$$v_r = f(\omega_1, \omega_2) \cdot (\cos\psi, \sin\psi) - \omega_3 r \qquad (7)$$

This component, $v_r$, is affine in $r$ along all the lines containing the image origin (Figure 3b). Considering $\omega_3 \neq 0$, $v_r$ vanishes when

$$r = \left(f\frac{\omega_1}{\omega_3}, f\frac{\omega_2}{\omega_3}\right) \cdot (\cos\psi, \sin\psi). \qquad (8)$$

Hence, the rotational component of the circular normal flow vanishes on a circle having the AOR and the image origin as diametrical opposite points.

Comparing equations (4) with (8) and equation (5) with (6), we conclude that the geometrical properties found for the radial and circular normal flow vectors are dual, as illustrated in Figure 3. In summary, the translational component of the radial / circular normal flow vanishes on the Γ-circle / Ψ-line, respectively. Additionally, the remaining rotational component is sinusoidal in $\psi$ or affine in $r$, respectively for the Γ-circle / Ψ-line.

Now, the representation of the radial and circular normal flow fields is remarkably simple in log-polar images: They correspond to the normal flow vectors that are respectively **horizontal** (along the log-polar coordinate $\lambda$), or **vertical** (along the log-polar coordinate $\gamma$). Thus, the application of the search algorithms, based on the circular normal flow or radial normal flow, seems quite natural in a log-polar geometry.

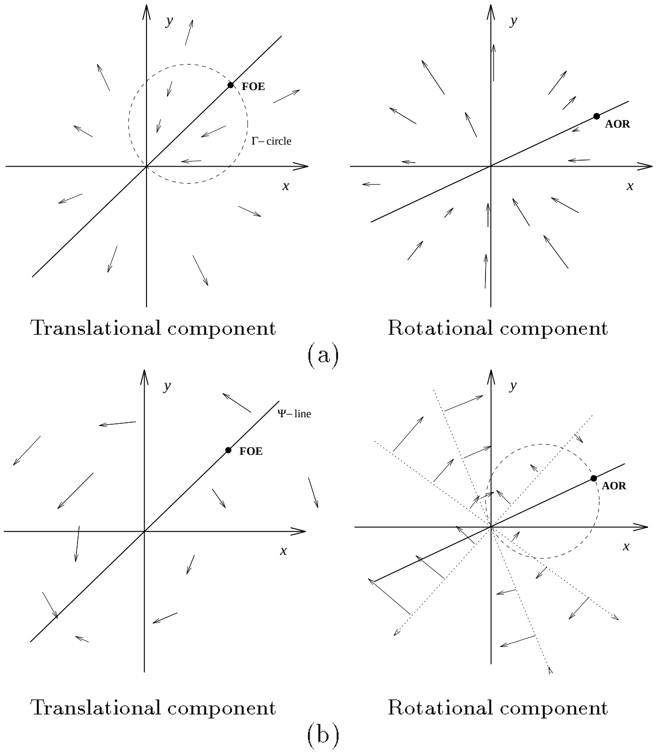


Figure 3: Geometric properties found for (a) radial and (b) circular normal flow vectors.

## 4.2 Constrained search algorithms

We have discussed before the geometric properties of the radial and circular normal flow and identified the images sites where the rotational and translational component are decoupled, thus allowing the estimation of the egomotion parameters. These properties suggest a set of search subspaces and corresponding algorithms. These search subspaces can be expressed on cartesian coordinates, as a function of a parameter $k$:

$$F(\mathbf{x};k) = 0 \tag{9}$$

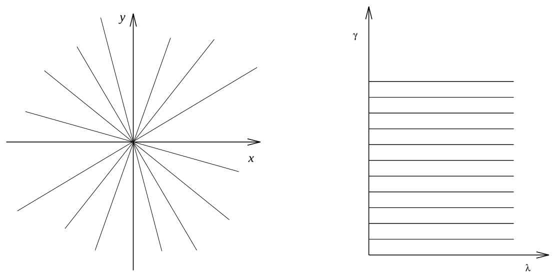


(a)

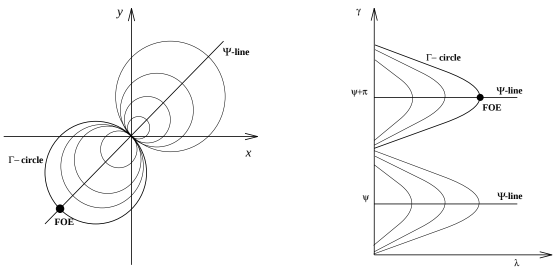


(b)

Figure 4: Constraints on cartesian and log-polar planes. a) Log-polar transformation from radial lines. b) Log-polar transformation from tangential circles.

The following examples show the two subspaces that we have defined.

- **Radial lines**: $F_r(\mathbf{x};k) = x\sin k + y\cos k$
- **Tangential circles**[1]: $F_c(\mathbf{x};k) = x^2 + y^2 - k(x\cos\Psi + y\sin\Psi)$.

Notice that the radial lines and the circles, described above, contain geometrical sites where the translational component of the normal flow vectors is zero, as shown in last section.

The geometrical constraints in cartesian coordinates can be modified to log-polar coordinates, performing a simple transformation (see Figure 4) :

$$\begin{cases} F_r(\mathbf{x};k) & \Rightarrow \quad F_r^*(\lambda,\gamma;k) = \gamma + k \\ F_c(\mathbf{x};k) & \Rightarrow \quad F_c^*(\lambda,\gamma;k) = \lambda - \log_l|\cos(\Psi-\gamma)| + k \end{cases}$$

[1]The function $F_c$ depends on a constraint on $\mathbf{\Sigma}$, defined by: $(\sigma,\eta)\cdot(-\sin\Psi,\cos\Psi) = 0$, and defines a set of circles containing the image center and having diameter $k$, along the $\Psi$-line defined in Section 4.1. The circle that contains the FOE corresponds to the $\Gamma$-circle.

Notice that the constraint on log-polar coordinates, described by $F_r^*(\lambda,\gamma;k) = 0$, represents horizontal lines of log-polar image.

For each subspace described above, there is an appropriate algorithm to compute a set of motion parameters, that suggests an adequate search strategy.

### 4.2.1 The $\Psi$-line algorithm

As described in Section 4.1, we can consider the *circular normal flow*, for each of the radial lines with orientation $\psi$:

$$\begin{aligned} U_\psi(r) &= \mathbf{n_C}\cdot\mathbf{v} = \\ &= -\rho(x,y)(\sigma,\eta)\cdot(-\sin\psi,\cos\psi) + \\ &+ f(\omega_1\cos\psi + \omega_2\sin\psi) - \omega_3 r \end{aligned} \tag{10}$$

where $r$ and $\psi$ denote the polar coordinates of the point $(x,y)$. The circular normal flow, $U_\psi$, is composed by an affine term in $r$, and a term that, in general, is non-linear in $r$. However, this non-linear component (the translational component) vanishes both when $\psi$ corresponds to the FOE direction (i.e. $\psi = \Psi$), or when the FOE is located at the image origin.

In log-polar coordinates, the rationale of the algorithm is to search an horizontal line $\psi^k$, such that the vertical flow, $U_\psi(r)$, is an affine function of $r$, as follows:

$$\min_{\hat{\psi}^k}\left\{\min_{\hat{p},\hat{\omega}_3}\left\{\boldsymbol{\mathcal{M}}\left(v_n - (p-\omega_3 r)|\psi^k\right)\right\}\right\}$$

where $p = f(\omega_1\cos\psi + \omega_2\sin\psi)$; $\boldsymbol{\mathcal{M}}(\mathbf{R}|\mathbf{D})$ expresses a measurement of the residuals $\mathbf{R}$ on a search domain $\mathbf{D}$, according to some metric (the mean of squares, the median of squares, etc). The search domain is the set of horizontal lines described by $F_r^*(\lambda,\gamma;k) = \gamma + k = 0$. For each line $\psi^k$, at least three points are needed to estimate $p$ and $\omega_3$, but more points are used to increase robustness. The direction corresponding to the FOE (the $\mathbf{\Psi}$-line) minimizes $\boldsymbol{\mathcal{M}}$.

A key aspect is that for the affine model fitting, we only use the image points where the normal flow vectors are aligned with the vertical direction of the log-polar images. The problem that remains to be solved is that of estimating the individual values of $\omega_1$, $\omega_2$, and the FOE, as only its direction, $\omega_3$ and a constraint on $\omega_1$ and $\omega_2$ are known.

### 4.2.2 The $\Gamma$-circle algorithm

Suppose that we had computed the *circular* normal flow to apply the $\mathbf{\Psi}$-line algorithm. In order to solve the remaining parameters, we can use the *radial* normal flow, $V_\psi(r) = \mathbf{n_r}\cdot\mathbf{v}$. In Section 4.1, we pointed out that the translational component of $V_\psi$ vanishes for every point on the $\Gamma$-circle. Given the known FOE-direction $\mathbf{\Psi}$, we can define the set of circles $\mathbf{\Gamma}^k$ containing the image center and having diameter $k$, along the $\mathbf{\Psi}$-line, described by the equation $F_c(\mathbf{x};k) = 0$ introduced in Section 4.1. Suppose that we compute $V_\psi(r)$

for the circle $\Gamma^k$ and divide both terms by $\frac{r^2}{f}+f$. Then we have, $\forall(x,y):\quad (x,y)\in\Gamma^k$,

$$\begin{aligned} T^k(\psi) &= \frac{V_\psi(r)}{\frac{r^2}{f}+f} = \\ &= \rho(x,y)\frac{r-(\sigma,\eta)\cdot(\cos\psi,\sin\psi)}{\frac{r^2}{f}+f} + \\ &+ \omega_1\sin\psi-\omega_2\cos\psi, \qquad (11) \end{aligned}$$

where r is dependent on $k$ and $\psi$, to ensure that $T^k(\psi)$ is computed on circle $\Gamma^k$.

We can conclude from (11) that if $\hat{\Gamma}^k$ corresponds to the $\Gamma$-circle, then $T^k(\psi)$ becomes sinusoidal in $\psi$. Based on this property, the algorithm consists in searching a circle[2] $\Gamma^k$, such that the flow along horizontal lines, $T^k(\psi)$, is sinusoidal in $\psi$. To estimate the sinusoidal parameters, we need two points, but more data are needed to find the $\Gamma$-circle. When approximating $T^k(\psi)$ to a sinusoidal function, the $\Gamma$-circle minimizes the following criterion:

$$\min_{\hat{\omega}_1,\hat{\omega}_2}\left\{\boldsymbol{\mathcal{M}}\left(\frac{v_n}{\frac{r^2}{f}+f}-(\omega_1\sin\psi-\omega_2\cos\psi)|\Gamma^k\right)\right\}$$

In this algorithm we only use the horizontal normal flow of the log-polar images to solve the remaining egomotion parameters, namely the FOE and the individual values of $\omega_1$ and $\omega_2$.

### 4.2.3 A sequential algorithm

In summary, our approach consists in a sequential algorithm with two steps. In the first step, the **$\Psi$-line search algorithm** uses vertical normal flow vectors and searches along horizontal lines to determine the FOE direction, $\omega_3$ and one constraint on $\omega_1$ and $\omega_2$. The second step of the sequential algorithm use the results provided by the $\Psi$-line algorithm and computes the remaining motion parameters, through the **$\Gamma$-circle search algorithm**. This algorithm uses horizontal normal flow vectors to search the $\Gamma$-circle. The process can be generalized for other algorithms applied for different search domains.

## 5 Results

The algorithm proposed here, was tested with synthetic and real images data. The synthetic image size is $256\times256$ pixels and the focal length, $f$, is 302 pixels. The real experiment image size is $322\times244$ pixels and the focal length is 229 pixels.

To apply a sequential estimation algorithm on the log-polar images, we have used a log-polar mapping of the images. Figure 5 illustrates the log-polar transformations, where $r_{min}=28.65$ pixels, the logarithmic factor $l=1.0151$, and the size of the resulting log-polar image is $180\times100$, for both sequences. Notice that the size of the log-polar images is roughly 4 times smaller than the original cartesian image size.

[2]In log-polar coordinates the $\Gamma^k$-circles do not correspond to circles (as shown in Figure 4), but by simplicity we keep the name of their cartesian correspondents.

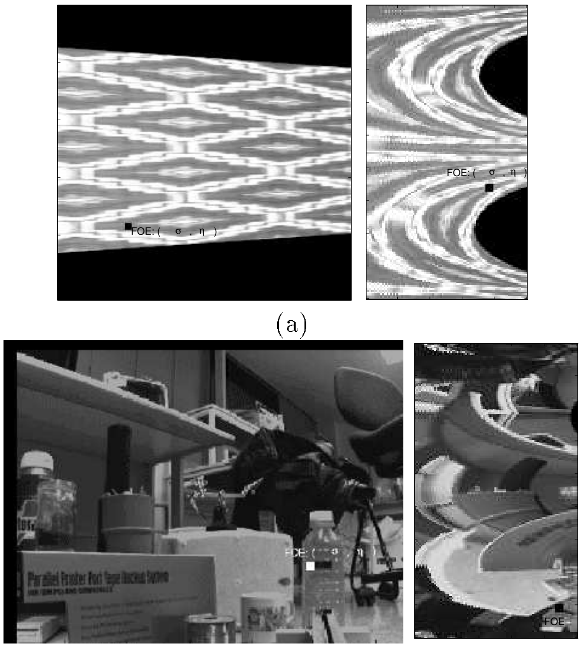

(a) (b)

Figure 5: Log-polar transformation.

In the synthetic sequence, the true location of the FOE is determined using the known motion parameters. In the real sequence, the true FOE is measured in the image by using known relevant points of the scene. The exact location of the FOE for each sequence is represented by a square mark in Figure 5.

In the first experiment, the camera rotates around the $Y$ axis at $-0.00785$ rad/frame, while translating. The $\Psi$-line and the $\Gamma$-circle algorithms were used to estimate the following rotational parameters: $(\omega_1,\ \omega_2,\ \omega_3)=(-0.001625,\ -0.008618,\ -0.000214)$ rad/frame. The true FOE in log-polar image is shown in Figure 6, together with the corresponding $\Psi$-line and $\Gamma$-circle found by the associated algorithms. The estimation errors seem large, due to the non-uniform image sampling effect, but the estimates are good approximations of the true values.

In the second experiment described here, the camera undergoes a pure translational motion in a real cluttered scene. The application of $\Psi$-line and the $\Gamma$-circle algorithms gives the following rotational estimation: $(\omega_1,\ \omega_2,\ \omega_3)=(0.00075, 0.00023, 0.0019)$ rad/frame, which are very small values, as expected. Similarly, by applying the $\Psi$-line and $\Gamma$-circle search algorithms the found line and circle intersect near to the true FOE, as shown in Figure 6.

We subdivided the search domain and the estimation problem, decreasing the complexity. In fact, the resulting computational time is significantly small. On

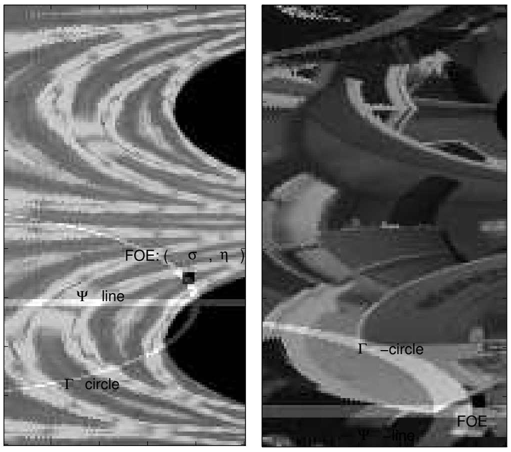


Figure 6: Estimation results from log-polar image using synthetic sequence (left) and real sequence (right).

the other hand, we apply the search algorithms on log-polar images (with less information). In spite of this, the results are very satisfactory and the egomotion estimates are good approximations of the true values.

## 6 Conclusions

In this paper, we addressed the problem of egomotion estimation for a monocular observer, moving under arbitrary 3D translation and rotation, using log-polar images.

As opposed to other approaches that consider the algorithmic aspects decoupled from the sensor geometry (or physiology), this work emphasizes the advantages of considering a visual problem both from a computational viewpoint and from sensor geometry specifications. In particular we have shown the advantages of using a log-polar image representation for the problem of egomotion estimation.

Apart from the use of the log-polar images, one of the most distinctive aspects of our approach is the use of spatio-temporal image derivatives, rather than the complete optical flow field. Furthermore, instead of using the whole set of image data, we consider only the image sites whose geometric properties convey relevant information about the observer motion.

Our method works in two successive steps. First, the **$\Psi$-line search algorithm** is used to determine the direction of the FOE, the rotation component around the $Z$ axis, and a linear constraint in the remaining two rotational components. In the second phase, we use the **$\Gamma$-circle search algorithm**, to determine completely the FOE, and the individual values of the angular velocity. These algorithms rely on the normal flow along **lines** or **columns** on the log-polar images, thus being remarkably well suited for this image representation.

For the $\Psi$-line algorithm, it is not required the presence of the FOE within the field of view, since the direction of the FOE can still be recovered. The $\Gamma$-circle algorithm can also be applied in this case, as parts of the $\Gamma$-circle will always be contained in the image. However, due to the limited image resolution, the estimation uncertainty will increase with the distance of the FOE to the image origin.

A number of experiments have been presented, for various kinds of motion, that illustrate the robustness of the approach. In the future, we plan to consider the constraints introduced by an active observer to improve the estimation processes and use the proposed methods for a closed loop navigation system.

## References

[1] Y. Aloimonos, I. Weiss, and A. Banddophaday. Active vision. *Int. Journal of Computer Vision*, 1(4):333–356, January 1988.

[2] A. Bernardino and J. Santos-Victor. Vergence control for robotic heads using log-polar images. In *Proc. of the IROS96*, Japan, November 1996.

[3] M. Bertero, T. Poggio, and V. Torre. Ill-posed problems in early vision. *Proceedings of the IEEE*, 76(8):869–889, 1988.

[4] K. Daniilidis and I. Thomas. Decoupling the 3d motion space by fixation. In *ECCV96*, Cambridge, UK, April 1996.

[5] C. Fermuller. Passive navigation as a pattern recognition problem. *Int. Journal of Computer Vision*, 14(2):147–158, March 1995.

[6] D. Heeger and A. Jepson. Subspace methods for recovering rigid motion i: Algorithm and implementation. *Int. Journal of Computer Vision*, 7(2):95–117, January 1992.

[7] B.K.P. Horn. *Robot Vision*. The MIT Press, 1986.

[8] B.K.P. Horn and E.J. Weldon. Direct methods for recovering motion. *International Journal of computer Vision*, 2(1):51–76, 1988.

[9] F. Lustman O. Faugeras and G. Toscani. Motion and structure from motion from point and line matches. In *Proc. 1st Intern. Conf. Comput. Vision*, London, June 1987.

[10] C. Silva and J. Santos-Victor. Robust egomotion estimation from the normal flow using search subspaces. Accepted for Publication by IEEE Trans. on PAMI, 1997.

[11] C. Silva and J. Santos-Victor. Direct egomotion estimation. In *Proc. of the 13th Int. Conf. on Pattern Recognition*, Vienna,Austria, August 1996.

[12] M. Tistarelli and G. Sandini. On the advantages of polar and log-polar mapping for direct estimation of the time-to-impact from optical flow. *IEEE Trans. on PAMI*, 15(8):401–411, April 1993.